Research Square

Preprints are preliminary reports that have not undergone peer review.
They should not be considered conclusive, used to inform clinical practice,
or referenced by the media as validated information.

Dynamic Contrast-Enhanced MRI Predicts *PTEN* Protein Expression which can Function as a Prognostic Measure of Progression-free survival in NPC patients.

Gang Wu
Hainan Medical College: Hainan Medical University
Weiyuan Huang
Hainan General Hospital
Wenzhu Li
Hainan General Hospital
Yu Wu
Hainan General Hospital
Qianyu Yang (yqy1026@163.com)
Hainan General Hospital https://orcid.org/0000-0001-8205-0500
Kun Liu
Hainan Medical College: Hainan Medical University
Mingyue Zhu
Hainan Medical College: Hainan Medical University
Priya S. Balasubramanian
Cornell University
Mengsen Li
Hainan Medical College: Hainan Medical University https://orcid.org/0000-0003-2512-0386

Research Article

Keywords: Phosphatase and tensin homolog deleted on chromosome ten, dynamic contrast-enhanced, magnetic resonance imaging, nasopharyngeal carcinoma, prognosis.

Posted Date: June 22nd, 2021

DOI: https://doi.org/10.21203/rs.3.rs-601565/v1

License: This work is licensed under a Creative Commons Attribution 4.0 International License.
Read Full License

Version of Record: A version of this preprint was published at Journal of Cancer Research and Clinical Oncology on August 16th, 2021. See the published version at https://doi.org/10.1007/s00432-021-03764-7.

Abstract

Objectives: The objective of our study was to investigate whether a phosphatase and tensin homolog deleted on chromosome 10 (*PTEN*) expression was associated with dynamic contrast-enhanced MRI (DCE-MRI) parameters and prognosis in nasopharyngeal carcinoma (NPC).

Methods: Two hundred and forty-five (245) patients with NPC who underwent pretreatment biopsy, PTEN immunohistochemistry of biopsy, and radical intensity-modulated radiation therapy (IMRT) with or without chemotherapy were included. Tumor segmentations were delineated on pretreatment MRI manually. The pharmacokinetic parameters (Ktrans, Kep, Ve, and Vp) derived from dynamic contrast-enhanced MRI (DCE-MRI) using the extended Toft's model within the tumor segmentations were estimated. The following demographics and clinical features were assessed and correlated against each other: gender, age, TNM stage, clinical-stage, Epstein-Barr virus (EBV), pathological type, progression-free survival (PFS), and prognosis status. DCE parameter evaluation and clinical feature comparison between the PTEN positive and negative groups was performed and correlation between PTEN expression with the PFS and prognosis status using Cox regression for survival analysis was assessed.

Results: A significantly lower K^{trans} and K_{ep} were found in NPC tumors in *PTEN* negative patients than in *PTEN* positive patients. K^{trans} performed better than K_{ep} in detecting *PTEN* expression with the ROC AUC of 0.752. *PTEN* negative was associated with later TNM stage, later clinical-stage, shorter PFS, and worse prognosis. Moreover, N stage, pathological type, K_{ep}, and prognostic status can be considered as independent variables in discrimination of *PTEN* negative expression in NPCs.

Conclusions: *PTEN* negative indicated a shorter PFS and worse prognosis than *PTEN* positive in NPC patients. K^{trans} and K_{ep} derived from DCE-MRI, which yielded reliable capability, should be considered as novel image markers that are correlated with *PTEN* expression and may be used to predict PTEN expression noninvasively. Combined radiological and clinical features can improve the performance of the classification of *PTEN* expression.

Introduction

Phosphatase and tensin homolog deleted on chromosome 10 (*PTEN*) is a tumor suppressor located on chromosome band 10q23 that regulates proliferation and differentiation in a variety of cancer cell types, including nasopharyngeal carcinoma (NPC) cells.[1,39] This locus encodes a dual-specificity phosphatase, with the *PTEN* protein has both lipid and protein phosphatase activity at its N-terminal domain, and a C-terminal C2 domain which can control cell migration in a calcium independent manner facilitated by the C-terminal PDZ-binding motif. [40] *PTEN* contains lipid phosphatase activity that regulates various cellular processes and signaling pathways, such as the induction of apoptosis through phosphatidylinositol 3-kinase (PI3K)/Akt pathway inhibition and control of cell adhesion, migration, and tumor invasion, by downregulating the activity of focal adhesion kinases (FAKs).[2,3] PTEN possesses a 50 amino acid C-terminal tail that is nonessential for activity but influences stability and can act to regulate and inhibit

PTEN functionality.[41] Inactivated or mutated *PTEN* also activates AMPK/mTOR/HIF1 pathway to promote angiogenesis and ultimately to promote the growth of NPC cells.[4] Inactivation of *PTEN* or low *PTEN* expression is associated with lymph node metastasis, advanced stage, and poor prognosis in NPCs.[5-7] Activation of *PTEN* may therefore be a promising approach for NPC tumor prevention and treatment target. Further, knowledge of a tumor possessing *PTEN* negative acquired mutations, being that this is an indicator of disease severity and progression, could help shape treatment regime.

Multiparametric MRI plays an important role in the detection, localization, staging, and predictive prognosis of NPC. The potential of various MRI techniques for the assessment of tumor aggressiveness and response to treatment regimes has recently been investigated.[8-10] Furthermore, as an integral part of clinical practice, MRI can characterize a diverse spectrum of tumoral phenotypes as potential biomarkers of genetic status. In particular, a sequence such as dynamic contrast-enhanced MRI (DCE-MRI) has the potential to provide parameters that may correlate and be predictive of levels of aggressiveness and genetic status of the tumor microenvironment.[10] Quantitative DCE-MRI parameters can be easily derived for each pixel within the tumor using commercially available software and can be visualized in a separate image for each parameter. This makes DCE-MRI a powerful prognostic tool. However, the genomic profiles underlying these images are not known, and the potential of quantitative DCE-MRI parameters as a surrogate or replacement for genomic markers and genetic assessment has not been extensively investigated with correlative and comparative biopsy tissue analysis. Imaging genomics is a novel field in cancer research that links and connects imaging parameters with genomic profiles. [8,11] Imaging methods that are found to be associated with gene expression patterns from tumor biopsies can then be used as noninvasive surrogate markers for genomic profiling and indicate potential information on tumor progression and prognosis.[12] K^{trans} derived from DCE has been shown to discriminate HIF expression level in NPC.[8,13] However, to our best knowledge, no study has been reported to focus on whether DCE can detect *PTEN* protein expression in NPC. Based on a previous knowledgebase and the following scientific hypothesis, we aim to explore the value of DCE in differentiating positive or negative *PTEN* expression in NPC patients and evaluate the correlation of *PTEN* expression status and clinical prognosis further.

Materials And Methods

Patients

All consecutive newly diagnosed NPC patients referred to the Department of Radiotherapy at Hainan General Hospital (The Affiliated Hainan Hospital of Hainan Medical University) between May 2018 and October 2020 were included in this prospective study approved by the hospital IRB (NO.2018025). All participating subjects were formally informed about the purpose of this study and a letter of consent was signed by every subject involved. The T, N, M, and clinical staging was performed according to the American Joint Committee on Cancer/Union for International Cancer Control (AJCC/UICC) staging system for NPC (8th edition, 2016).[14] Patients met the inclusion criteria by (1) having

Karnofsky performance status ≥70%, (2) having NPC as confirmed by biopsy and histopathology, (3) performed *PTEN* immunohistochemical staining before treatment, and (4) having undergone DCE-MRI before treatment in our hospital. Patients were excluded if they (1) had MRI (eg, artificial cochlea, cardiac pacemaker implantation) or radiotherapy contraindications, (2) Failure to complete treatment or loss of follow-up less than 3 months, (3) had previously received radiotherapy in the neck region, (4) had any other malignant tumors in the prior 5 years, or (5) suffered from severe neurological or psychiatric diseases.

Clinical endpoints were progression-free survival (PFS) for follow-up status assessed on 1 Jan 2021, using the last MR follow-up as the endpoint. For PFS, time from diagnosis to disease-related death, the first event of relapse, or clinical follow-up endpoint was used. Patients suffering from disease-related death or relapse were categorized under “poor prognosis”, others categorized under “good prognosis”.

Treatment regimen

The choice of treatment regimen according to National Comprehensive Cancer Network (NCCN) Guidelines (https://www.nccn.org/).[15] All patients were treated by radical three-dimensional conformal and intensity-modulated radiation therapy (IMRT). Radiotherapy was completed using the following equipment: three-dimensional treatment planning system (Eclipse, American), 3000A mobile laser positioning system (Gammex A), Trilogy medical linear accelerator 6MVX line (Varian), 16-slice spiral CT (Siemens), supporting vacuum bag fixing device, and three-dimensional fixing frame. The patients were in a supine position and fixed with a thermoplastic memory membrane in the head and neck. Positioning CT was performed using a thin-layer continuous scanning scheme with 3 mm thickness, tube voltage 140kV, current 280mAs. The images were input into Eclipse three-dimensional treatment planning system. The range of tumors was determined by MR images, and the target area was delineated and planned by fused MR and positioning CT images. The planning target volume (PTV) formed by expanding 3-5mm from each target area was administered a prescription dose: nasopharyngeal tumor volume (GTVnx) and cervical lymph node volume (GTVnd) at 66-73 Gy and 63-70 Gy, respectively; high-risk area of primary focus (CTV1) at 62-64 Gy; low-risk area of primary focus and cervical lymph node drainage area (CTV2) at 54-58 Gy; PTV1 and PTV2 at 54 Gy and 50 Gy, respectively. The number of segmentations was 31-35 times, 5 times per week.

Induction chemotherapy consisted of Docetaxel and Cisplatin and were given at 75 mg/m^2 intravenously on day 1, or 25 mg/m^2 intravenously on days 1-3, once per 3 weeks lasting for 2 to 4 rounds. Concurrent Chemotherapy consisted of Cisplatin 75 mg/m^2 on day 1 (or 25 mg/m^2 days 1-3) once per 3 weeks.

Follow-up assessments were performed every 3 months for the first year, every 6 months for years 2-5, then every year subsequently. Routine follow-up assessments included assessment of vital signs and any adverse events. MR scans were done at every follow-up time point.

MRI acquisition

MRI examinations were performed on a 3.0-T scanner (Skyra, Siemens Medical Solutions, Erlangen, Germany), equipped with a 20-channel sensitivity-encoding combined head and neck coil. Patients underwent routine MRI, including T1-weighted spin-echo sequence (field of view [FOV], 180×180 mm^2; section thickness, 4 mm; repetition time [TR]/echo time [TE], 625/9.0 milliseconds), T2-weighted fast spin-echo sequence (FOV, 180×180 mm^2; section thickness, 4 mm; TR/TE, 4070/30 milliseconds). Baseline T1-mapping was obtained before DCE-MRI with 5 different flip angles, including 3°, 6°, 9°, 12°, and 15°, using a fast low angle shot (FLASH)/vibe sequence. All other parameters were held constant as the following - DCE-MRI was performed with a (FLASH)/vibe sequence, 50 dynamic acquisitions, 4.9 seconds per dynamic acquisition, with the following parameters: TR/TE, 4.09/1.47 milliseconds; flip angle, 9; matrix, 192×144; FOV, 180×180 mm^2; section thickness, 4 mm; phase, 75%; bandwidth, 400 Hz. Contrast enhancement was performed with a standard 0.1 mmol/kg body weight dose of gadolinium-based contrast agent of Gadodiamide (Omniscan, GE Medical Systems, Amersham, Ireland). The gadolinium-based contrast agent was administered through a catheter in the antecubital vein by an automatic power injector (Medrad, Pittsburgh, Pennsylvania, USA) at a rate of 2 mL/second and was followed by a double bolus injection of isotonic saline. The dynamic acquisition was performed with a temporal resolution of 4.9 seconds, and the contrast agent was administered after 5 baseline dynamics. After the DCE-MRI, contrast-enhanced T1-weighted spin-echo sequences were conducted on axial, coronal, and sagittal planes.

MRI post-processing and analysis.

DCE-MRI data were analysed using the OmniKinetics (OK) software (GE Pharmaceutical). The DCE parameters (K^{trans}, reflux rate [K_{ep}], the volume fraction of the extravascular extracellular matrix [V_e], and blood plasma volume [V_p]) were estimated using the extended Toft's two-compartment model[16] and population-averaged AIF.[17]

Two independent radiologists, (readers I (Weiyuan) and II (Wenzhu); 12 and 5 years of experience in MRI, respectively), who were blinded to clinical information, performed tumor segmentation to encompass whole tumor volume on anatomic reference images; among axial T1WI, PdWI, and post-contrast T1WI. Reference image and DCE parameter maps were loaded into a multimodality tumor tracking application ITK-SNAP (version 3.4.0, USA, http://www.itksnap.org). [18] The regions of interest (ROIs) drawn on the anatomic reference images were simultaneously mapped to the corresponding location on the DCE parameter maps. The mean values of K^{trans}, K_{ep}, V_e, and V_p from the volumetric ROIs were recorded for correlations and analysis.

PTEN protein expression detecting by immunohistochemistry

In every patient, the diagnosis was confirmed by tumor biopsy. The pathological type was classified according to the cell type and degree of differentiation: undifferentiated non-keratinized carcinoma, differentiated non-keratinized carcinoma, or keratinizing squamous cell carcinoma.[19] Immunohistochemistry for PTEN protein was performed for all obtained biopsies for all cases used in

this study, and the loss of protein expression was defined as an absence of cytoplasmic staining around a counterstained nucleus. Positive controls were obtained on a per biopsy basis from surrounding unaffected stroma and vasculature. After tissue sections were deparaffinized and rehydrated, tissue was sectioned into 4 μm thick slices were treated with antigen retrieval buffer (S1699, Dako) in a steamer for 20 minutes. Anti-PTEN antibody (100 μL [product number 9188, Cell Signaling Technology]) was applied to tissue sections for overnight incubation at 4°C in a humidity chamber. After a Tris-buffered saline (PBS) wash, tissue sections were incubated with biotinylated monoclonal anti-rabbit IgG (100 μL [product number ZA-0635, ZSGB-BIO]) for 20 minutes at 37℃. The antigen-antibody binding was detected by a kit (Vectastain Elite ABC kit, product number PK-6100, Vector Laboratories) and a DAB (3, 3-diaminobenzidine) system (product number K3468, Dako). Tissue sections were briefly immersed in hematoxylin for counterstaining and were covered with cover glasses. PTEN expression was scored by the pathologist (Y.W.) based on the percentage of positive staining tumor cells (Nucleus/cytoplasm). PTEN staining in the adjacent stroma and blood vessels served as a positive internal control, due to heterogeneity within the tumor focus. To account for this heterogeneity, foci were scored as PTEN-positive (≥95% cancer cells positive), and PTEN-negative (<5% cancer cells positive) (Figure 1).

Statistical analysis.

Patients' characteristics were compared between the *PTEN* positive and *PTEN* negative groups. Continuous variables were analyzed using the independent sample *t-test* or *Mann-Whitney U* test, and categorical variables were analyzed using a *chi-square test* or *Fisher's exact test* according to the data distribution, respectively. For continuous variables with a *p*-value less than 0.20, a receiver operating characteristic (ROC) curve was constructed and the area under the curve (AUC) was calculated. Optimal cutoff points were determined based on the maximum Youden index. Spearman correlation analyses (correlation coefficient, ρ) were performed to assess the correlation between *PTEN* positive or negative and clinical or radiographic features. Cox survival analyses were performed to evaluate the prognostic significance of *PTEN* expression in NPC patients. DCE parameters' values, gender, age, EBV, T, N, M stage, PFS, and prognosis status were used as covariates to evaluate the independent detecting value of the classifier using multiple variables logistic regression.

Interobserver agreement between reader I and II was assessed using the intraclass correlation coefficient (ICC). An ICC of 1.0 was considered to represent perfect agreement; 0.81-0.99, almost perfect agreement; 0.61-0.80, substantial agreement; 0.41-0.60, moderate agreement; 0.21-0.40, fair agreement; and 0.20 or less, slight agreement.[28]

All statistical analyses and graphing were performed using Prism GraphPad Software version 9.0 (GraphPad Software, La Jolla, CA, USA. https://www.graphpad.com/scientific-software/prism/), and a *p*-value less than 0.05 was considered statistically significant.

Results

Demographics and Clinical Features

A total of 273 NPC patients were enrolled. After verifying exclusion criteria, 245 patients remained. The mean age was 50.09 (±11.41) years old, 65.31% males. The *PTEN* expression type accounted for 87.35% of patients with positive, whereas 12.65% corresponded to negative (Figure 1). T, N, M stage and clinical-stage showed a significant difference between the *PTEN* positive and *PTEN* negative groups in comparison of demographic and clinical features (Table 1). Regarding EBV, 73.47% of patients suffered from positive, and 26.53% suffered from negative (Table 1). *PTEN* positive was associated significantly negatively with T, N, M, and clinical-stage among demographics and clinical features in NPC patients. *PTEN* positive was in 93.75% (15/16) of clinical stage II, 91.67% (110/120) of stage III, 84.95% (79/93) of stage IVA tumors, and 62.5% (10/16) of stage IVB tumors.

PTEN expression correlated with DCE-MRI

Interobserver agreements were as follows; K^{trans} ICC=0.915, 95% confidence interval [CI]: 0.823-0.964; K_{ep} ICC=0.973, 95% CI: 0.922-0.989; V_e ICC=0.993, 95% CI: 0.978-0.996; V_p ICC=0.998, 95% CI: 0.994-0.999. Because the measurements of all MRI parameters showed almost perfect interobserver agreement, the average of both readers' measurements were used. K^{trans} (p<0.001) and K_{ep} (p<0.001) were significantly lower in *PTEN* positive group than *PTEN* negative group. V_e (p<0.994) and V_P (p<0.074) could not distinguish *PTEN* positive from negative. Spearmen correlation analyses also confirmed the same results. *PTEN* expression type was associated significantly with K^{trans} (ρ=-0.290, p<0.001) and K_{ep} (ρ=-0.241, p<0.001) (Table 2, Figure 2). ROC analysis showed K^{trans} distinguishing *PTEN* positive from negative with an AUC of 0.752 (95% CI, 0.674-0.829), an 80.65% sensitivity, a 60.75% specificity using 0.85 as the cutoff. K_{ep} performed worse than K^{trans} for classifying *PTEN* expressions with an AUC of 0.629 (95% CI, 0.524-0.734), a 64.52% sensitivity, a 62.62% specificity using 2.068 as the cutoff (Figure 3). Representative cases of *PTEN* positive and *PTEN* negative groups were shown in Figure 2.

PTEN positive associated with better prognosis than *PTEN* negative NPCs

The prognostic significance of the *PTEN* expression type was evaluated based on the PFS of NPC patients. In the *PTEN* negative group, a significantly shorter PFS, and lower cumulative incidence of recurrence and death have observed (Table 1 and Figure 3).

Multiple variables logistic regression results are based on multivariate analysis using N stage, pathological type, K_{ep} and prognostic status considered as associated variables from the earlier section analysis in the classification of *PTEN* expression. The multivariable logistic regression model has a good performance in detecting *PTEN* expression with an AUC of 0.843 (95% CI, 0.762-0.924), a 84.62% negative predictive power, and a 91.38% positive predictive power (Figure 3).

Discussion

Accumulating evidence suggests that *PTEN* is an independent prognostic factor in patients with NPC; *PTEN* negative patients are more likely to have worse prognosis. Considering its prognostic significance, this pilot study implemented a comparison with quantitative parameters derived from DCE-MRI firstly, which accurately correlates with and thus predicts *PTEN* expressions in NPC. This study further confirms that *PTEN* negative indicates a shorter PFS and worse prognosis than *PTEN* positive NPC patients. The multivariable regression model combined clinical and image features could provide more accurate predictability of *PTEN* expression.

PTEN is one of the tumor suppressors whose positive expressions have been found in head and neck squamous cell carcinoma (HNSCC) commonly, with low negative rates of approximately 10-30%.[20,21] Our dataset showed 87.35% positive and 12.65% negative *PTEN* in NPCs, with an expression rate close to HNSCC. The reported *PTEN* positive rates of other types of malignant tumors, such as colorectal cancer[22] or prostate cancer,[23] were lower than NPCs. This may be a contributing factor to the longer five-year survival rate and overall survival of NPC patients than other common types of malignancies.

T, N, M stage, and clinical-stage showed a significant difference between the *PTEN* positive and negative groups among all demographic and clinical features. We demonstrated that higher TNM or clinical stages have a higher *PTEN* negative rate in NPC tumors. This suggests that *PTEN* has a significant contribution to TNM stage and clinical-stage in NPC tumors. Previous studies reveal similar results regarding either NPC,[7] or colorectal cancer,[2] gastric cancer,[24] and hepatocellular carcinoma.[25] Several studies showed protein expression of *PTEN* was low in EBV positive NPC.[26,27] Our study shows that expression of *PTEN* did not show a significant difference between the EBV positive and negative groups of NPC patients, needing further study to confirm. This inconsistent result could be due to the small number of patients in the subgroup of negative EBV and *PTEN* in NPCs in our study.

Additionally, we explore the value of DCE in differentiating *PTEN* positive from *PTEN* negative status in NPC patients. DCE-MRI can quantitatively characterize tumor perfusion and is associated with microvessel density and permeability. Several studies have reliably estimated hypoxia-inducible factor-1 (HIF-1α), epidermal growth factor receptor (EGFR), or vascular endothelial growth factor (VEGF) expression via DCE-MRI quantitatively parameters in HNSCC,[11,28] including NPC.[8,13] It has been shown that different DCE parameters reflected different aspects of tumor microstructure.[29,30] As the functionality of PTEN is that of a tumor suppressor which is known to influence cell migration, growth rate regulation, and various other processes that lead to tumorigenesis, it is likely that the pathways that are altered due to PTEN negative status cause definite and drastic tumor microenvironmental changes that are gathered by DCE-MRI and can be predictive of PTEN status. At present, we found that K^{trans} and K_{ep} derived from DCE Toft's model had the discriminative ability to detect *PTEN* expression status. K^{trans} (min^{-1}) reflects contrast agent flow from the vascular space to the extravascular extracellular space (EES), which was the most commonly used parameter in Toft's model, representing vessel permeability.[29,30] Prior studies have correlated K^{trans} to measures of tumor vessel permeability or oxygenation levels such as HIF-1α.[8] Referring to our results, we speculate that, without the inhibition of the suppressor gene

PTEN, angiogenesis and aggressiveness of tumors increase significantly. The high permeability of immature neovascular probably caused the increase of K^{trans} in NPCs. K_{ep} (min^{-1}) is the reverse reflux rate constant between the extracellular space and plasma and is equal to K^{trans}/V_e. A recent study by Stephanie M. McCann et al [31] reported there was a significant negative correlation between K_{ep} and *PTEN* expression in prostate cancer. However, Marta D Switlyk et al [32] reported that DCE can not discriminate *PTEN* expression in prostate cancer. Significant heterogeneity of prostate cancer may be the reason for this disagreement. NPCs were a homogeneous undifferentiated small round cell solid tumor, tending to have high cellularity and low possibility of necrosis. DCE-MRI might be more suitable for small round cell solid tumors, such as NPC, to evaluate angiogenesis or oncogene/suppressor gene expression. V_e might be strongly associated with cellularity because it reflects the amount of extracellular space, as it was exemplarily shown in a glioma model. [33] V_p is defined as the blood per unit volume of tissue recommended as an alternative imaging biomarker for the assessment of blood volume.[34] Our results showed that V_e and V_p having limited discriminative ability in predicting *PTEN* expression, indicating no significant difference in cellularity among NPC tumors with different degrees of angiogenesis and aggressiveness. The failure of the significant correlation between V_p and *PTEN* may be explained by the fact that high vascular permeability induced by inactivation of *PTEN* can result in a high interstitial pressure in a tumor, which may make microvasculature distort, deform, collapse, and even divert. [35,36] This will reduce the effective blood flow and limit the volume of contrast agent distribution. Di et al [36] also fail to detect VEGF expression using V_p derive from DCE-MRI. Our ROC analysis showed K^{trans} has a larger AUC than K_{ep}. However, multivariable logistic regression reveals that only K_{ep} out of DCE parameters acts as an independent detecting factor. This result could be due to underlying distributional differences. K_{ep} was analyzed under assumption of normal distribution, however, K^{trans} is not normally distributed. Future research will perform further statistical tests by employing data normalization techniques and standardization across parameters to derive more accurate parameter relatedness.

Furthermore, we evaluate the correlation of *PTEN* expression status and prognosis and build the multiple variable logistic regression model to assess independent detecting metrics. Several studies have suggested that *PTEN* mutant/loss function could serve as a prognostic factor in head and neck malignant tumors[20,21], including NPC[37,38]. Our results were comparable to previous studies, *PTEN* positive NPCs demonstrated a longer PFS and better prognosis status than *PTEN* negative NPCs using cox survival analysis. Considering NPC has a much higher 5-year survival rate and a better prognosis than other malignant tumors, we defined the clinical endpoint indicating a poor prognosis as either recurrence, metastasis, or death rather than only death during the follow-up. 32 out of 214 *PTEN* positive NPC patients suffering from a poor prognosis, while 9 out of 31 *PTEN* negative NPC patients suffering from a poor prognosis. Multiple variable logistic regression showed the N stage, pathological type, K_{ep} and prognostic status can considered as independent variables in the classification of *PTEN* expression. We confirmed that combined clinical and radiological features can improve the performance of

discrimination of *PTEN* expression as positive or negative in NPC patients. N stage is a stronger independent variable than T stage which may be related to *PTEN* inducing lymph node metastasis.[5,6]

There are a few limitations in this study. Due to the inherent rarity of *PTEN* negative in NPC, there is an imbalance of sample size between the two groups. We used a suitable analysis model and correction according to the data distribution to minimized sample size imbalance. Moreover, *PTEN* expressions were determined by immunohistochemical rather than sequencing due to a lack of available data. Further studies are needed to verify our results using PCR sequencing. Following this sequencing, it will be important to understand the underlying mutation in *PTEN* that leads to a nonfunctional phenotype, as C-terminal tail deletion could actually enhance *PTEN* activity, while many mutations may reduce or remove activity. Comparisons between nascent RNA, mRNA, and DNA sequence in addition to transcript levels will determine the specific form and role of the mutation. There could be a potential upregulation of *PTEN* in *PTEN* positive tumors that could act as protective. Thus comparisons between *PTEN* expression levels between the tumor tissue and control tissue from the same patient will be illuminating towards potential *PTEN* upregulation. Genome screening will be implemented in future clinical studies in order to determine whether inherited *PTEN* mutations exist in patients or the vast majority, as expected, are acquired mutations. Further, extracellular *PTEN* uptake is possible and further influenced by tissue order and heterogeneity.[42] Thus in the case of heterogeneous *PTEN* expression due to acquired mutation, the localization of *PTEN* positive cells could act as protective to nearby cells if *PTEN* is further upregulated. Future biopsy sections will be imaged to detect differences in nuclear and cytoplasmic localization of *PTEN*, along with sequencing data that will unveil mutation type, as cellular localization changes of *PTEN* could be another prognostic indicator.[43] Additionally, a relatively short follow-up period makes it impossible for us to evaluate the correlation of *PTEN* expressions and five-year survival rate or long-term prognosis.

In conclusion, the current study applied DCE-MRI to detecting *PTEN* expression noninvasively in NPC patients. Among DCE quantitative parameters, K^{trans} and K_{ep}, which yielded reliable capability in predicting *PTEN* expression, should be considered as novel predictive image markers. Furthermore, combined clinical and imaging features can improve the performance of classification of *PTEN* status. *PTEN* negative expression predicts a less favorable survival outcome in patients with NPC.

Declarations

Funding

This work was supported by the Key Research and Development Program of Hainan Province (ZDYF2019137) and the National Natural Science Foundation of China (grant nos. 81660285 and 81871346).

Conflicts of Interest

The authors declare that there are no conflicts of interest.

Availability of data and material

All datasets generated or analysed during this study are included in this published article and its supplementary information files.

Code availability

Not applicable.

Authors' Contributions

Conceptualization was done by Gang Wu. Data curation was performed by Gang Wu, Weiyuan Huang, Wenzhu Li, and Qianyu Yang. Pathology analysis was conducted by Yu Wu. Formal analysis was conducted by Weiyuan Huang. Investigation was performed by Gang Wu, Weiyuan Huang, Wenzhu Li, Qianyu Yang, and Kun Liu. Methodology was contributed by Gang Wu, Weiyuan Huang, Mingyue Zhu, and Mengseng Li. Project administration was done by all the authors. Visualization was performed by Weiyuan Huang. Supervision was done by Mengseng Li. Writing of the original draft was performed by Gang Wu. Writing in terms of review and editing was performed by Mengseng Li, Mingyue Zhu, and Weiyuan Huang.

Ethics approval

This prospective study was approved by Hainan General Hospital (The Affiliated Hainan Hospital of Hainan Medical University) IRB (NO.2018025).

Consent to participate

All participating subjects were formally informed about the purpose of this study and a letter of consent was signed by every subject involved.

Consent for publication

Written informed consent was obtained from the patient for publication and any accompanying images.

Acknowledgments

We would like to thank all the patients and the personnel involved in this study. We are also grateful to Ganmian Dai and Tiansheng Li at the Radiology Department, the Hainan General Hospital, for help in data collation.

References

1. Aquila S, Santoro M, Caputo A, Panno ML, Pezzi V, De Amicis F. The Tumor Suppressor PTEN as Molecular Switch Node Regulating Cell Metabolism and Autophagy: Implications in Immune System and Tumor Microenvironment. *Cells.* 2020;9(7)
2. Kim B, Kang SY, Kim D, Heo YJ, Kim KM. PTEN Protein Loss and Loss-of-Function Mutations in Gastric Cancers: The Relationship with Microsatellite Instability, EBV, HER2, and PD-L1 Expression. *Cancers (Basel)*. 2020;12(7)
3. Lyu J, Yu X, He L et al (2015) The protein phosphatase activity of PTEN is essential for regulating neural stem cell differentiation. Mol Brain 8:26
4. Lyu X, Wang J, Guo X et al (2018) EBV-miR-BART1-5P activates AMPK/mTOR/HIF1 pathway via a PTEN independent manner to promote glycolysis and angiogenesis in nasopharyngeal carcinoma. PLoS Pathog 14(12):e1007484
5. Cai LM, Lyu XM, Luo WR et al (2015) EBV-miR-BART7-3p promotes the EMT and metastasis of nasopharyngeal carcinoma cells by suppressing the tumor suppressor PTEN. Oncogene 34(17):2156–2166
6. Cai L, Ye Y, Jiang Q et al (2015) Epstein-Barr virus-encoded microRNA BART1 induces tumour metastasis by regulating PTEN-dependent pathways in nasopharyngeal carcinoma. Nat Commun 6:7353
7. Xu X, Yang H, Huo X (2004) [Expression and significance of PTEN in nasopharyngeal carcinoma]. Lin Chuang Er Bi Yan Hou Ke Za Zhi 18(11):658–659
8. Liu L, Hu L, Zeng Q et al (2021) Dynamic contrast-enhanced MRI of nasopharyngeal carcinoma: correlation of quantitative dynamic contrast-enhanced magnetic resonance imaging (DCE-MRI) parameters with hypoxia-inducible factor 1alpha expression and tumor grade/stage. Ann Palliat Med 10(2):2238–2253
9. Zhang B, Tian J, Dong D et al (2017) Radiomics Features of Multiparametric MRI as Novel Prognostic Factors in Advanced Nasopharyngeal Carcinoma. Clin Cancer Res 23(15):4259–4269
10. Huang B, Wong C-S, Whitcher B et al (2013) Dynamic contrast-enhanced magnetic resonance imaging for characterising nasopharyngeal carcinoma: comparison of semiquantitative and quantitative parameters and correlation with tumour stage. European Radiology 23(6):1495–1502
11. Meyer HJ, Leifels L, Hamerla G, Hohn AK, Surov A (2019) Associations between Histogram Analysis Parameters Derived from DCE-MRI and Histopathological Features including Expression of EGFR, p16, VEGF, Hif1-alpha, and p53 in HNSCC. Contrast Media Mol Imaging 2019:5081909
12. Xie Q, Wu J, Du Z et al (2019) DCE-MRI in Human Gliomas: A Surrogate for Assessment of Invasive Hypoxia Marker HIF-1A Based on MRI-Neuronavigation Stereotactic Biopsies. Academic Radiology 26(2):179–187
13. Surov A, Meyer HJ, Hohn AK, Sabri O, Purz S (2019) Combined Metabolo-Volumetric Parameters of (18)F-FDG-PET and MRI Can Predict Tumor Cellularity, Ki67 Level and Expression of HIF 1alpha in Head and Neck Squamous Cell Carcinoma: A Pilot Study. Transl Oncol 12(1):8–14

14. Amin MB, American Joint Committee on Cancer (2016) AJCC cancer staging manual, 8th edn. Springer, New York
15. Colevas AD, Yom SS, Pfister DG et al (2018) NCCN Guidelines Insights: Head and Neck Cancers, Version 1.2018. J Natl Compr Canc Netw 16(5):479–490
16. Tofts PS, Brix G, Buckley DL et al (1999) Estimating kinetic parameters from dynamic contrast-enhanced T(1)-weighted MRI of a diffusable tracer: standardized quantities and symbols. J Magn Reson Imaging 10(3):223–232
17. Huang B, Wong C-S, Whitcher B et al (2013) Dynamic contrast-enhanced magnetic resonance imaging for characterising nasopharyngeal carcinoma: comparison of semiquantitative and quantitative parameters and correlation with tumour stage. European radiology 23(6):1495–1502
18. Yushkevich PA, Piven J, Hazlett HC et al (2006) User-guided 3D active contour segmentation of anatomical structures: significantly improved efficiency and reliability. Neuroimage 31(3):1116–1128
19. Shi S, Cao X, Gu M, You B, Shan Y, You Y. Upregulated expression of SOX4 is associated with tumor growth and metastasis in nasopharyngeal carcinoma.(Research Article)(superoxide dismutase 4)(Report). 2015;2015
20. Pfisterer K, Fusi A, Klinghammer K, Knodler M, Nonnenmacher A, Keilholz U (2015) PI3K/PTEN/AKT/mTOR polymorphisms: association with clinical outcome in patients with head and neck squamous cell carcinoma receiving cetuximab-docetaxel. Head Neck 37(4):471–478
21. da Costa A, Costa FD, Araujo DV et al (2018) The roles of PTEN, cMET, and p16 in resistance to cetuximab in head and neck squamous cell carcinoma. Med Oncol 36(1):8
22. Li FH, Shen L, Li ZH et al (2010) Impact of KRAS mutation and PTEN expression on cetuximab-treated colorectal cancer. World J Gastroenterol 16(46):5881–5888
23. Eineluoto JT, Sandeman K, Pohjonen J et al. Associations of PTEN and ERG with Magnetic Resonance Imaging Visibility and Assessment of Non-organ-confined Pathology and Biochemical Recurrence After Radical Prostatectomy. *Eur Urol Focus*. 2020
24. Wen YG, Wang Q, Zhou CZ, Qiu GQ, Peng ZH, Tang HM (2010) Mutation analysis of tumor suppressor gene PTEN in patients with gastric carcinomas and its impact on PI3K/AKT pathway. Oncol Rep 24(1):89–95
25. Fu X, Wen H, Jing L et al (2017) MicroRNA-155-5p promotes hepatocellular carcinoma progression by suppressing PTEN through the PI3K/Akt pathway. Cancer Sci 108(4):620–631
26. Wu Q, Han T, Sheng X, Zhang N, Wang P (2018) Downregulation of EB virus miR-BART4 inhibits proliferation and aggressiveness while promoting radiosensitivity of nasopharyngeal carcinoma. Biomed Pharmacother 108:741–751
27. Peng H, Chen Y, Gong P et al (2016) Higher methylation intensity induced by EBV LMP1 via NF-kappaB/DNMT3b signaling contributes to silencing of PTEN gene. Oncotarget 7(26):40025–40037
28. Donaldson SB, Betts G, Bonington SC et al (2011) Perfusion estimated with rapid dynamic contrast-enhanced magnetic resonance imaging correlates inversely with vascular endothelial growth factor

expression and pimonidazole staining in head-and-neck cancer: a pilot study. Int J Radiat Oncol Biol Phys 81(4):1176–1183

29. Yuan J, Chow SK, Yeung DK, Ahuja AT, King AD (2012) Quantitative evaluation of dual-flip-angle T1 mapping on DCE-MRI kinetic parameter estimation in head and neck. Quant Imaging Med Surg 2(4):245–253
30. Nejad-Davarani SP, Bagher-Ebadian H, Ewing JR et al. An extended vascular model for less biased estimation of permeability parameters in DCE-T1 images. *NMR Biomed.* 2017;30(6)
31. McCann SM, Jiang Y, Fan X et al (2016) Quantitative Multiparametric MRI Features and PTEN Expression of Peripheral Zone Prostate Cancer: A Pilot Study. AJR Am J Roentgenol 206(3):559–565
32. Switlyk MD, Salberg UB, Geier OM et al. PTEN Expression in Prostate Cancer: Relationship With Clinicopathologic Features and Multiparametric MRI Findings. *AJR Am J Roentgenol.* 2019:1–9
33. Ozturk K, Soylu E, Tolunay S, Narter S, Hakyemez B (2019) Dynamic Contrast-Enhanced T1-Weighted Perfusion Magnetic Resonance Imaging Identifies Glioblastoma Immunohistochemical Biomarkers via Tumoral and Peritumoral Approach: A Pilot Study. World Neurosurg 128:e195–e208
34. Artzi M, Liberman G, Nadav G et al (2015) Human cerebral blood volume measurements using dynamic contrast enhancement in comparison to dynamic susceptibility contrast MRI. Neuroradiology 57(7):671–678
35. DeVries AF, Kremser C, Hein PA et al (2003) Tumor microcirculation and diffusion predict therapy outcome for primary rectal carcinoma. Int J Radiat Oncol Biol Phys 56(4):958–965
36. Di N, Cheng W, Jiang X et al (2019) Can dynamic contrast-enhanced MRI evaluate VEGF expression in brain glioma? An MRI-guided stereotactic biopsy study. J Neuroradiol 46(3):186–192
37. Hu Z, Zhou S, Luo H et al (2019) miRNA-17 promotes nasopharyngeal carcinoma radioresistance by targeting PTEN/AKT. Int J Clin Exp Pathol 12(1):229–240
38. Li DP, Chai W, Liu YH, Xu TT, Huang H (2019) MicroRNA-142 promotes the development of nasopharyngeal carcinoma through targeting PTEN. Eur Rev Med Pharmacol Sci 23(9):3806–3812
39. Rasheed BK, Ahmed et al. "PTEN gene mutations are seen in high-grade but not in low-grade gliomas." Cancer research57.19 (1997): 4187–4190
40. Raftopoulou M et al (2004) "Regulation of cell migration by the C2 domain of the tumor suppressor PTEN. " Science 303(5661):1179–1181
41. Vazquez F et al (2000) Phosphorylation of the PTEN tail regulates protein stability and function. Molecular cellular biology 20(14):5010–5018
42. Putz U, Mah S, Goh CP, Low LH, Howitt J, Tan SS. PTEN secretion in exosomes. Methods. 2015 May;77–78:157 – 63
43. Bononi A, Pinton P (2015 May) Study of PTEN subcellular localization. Methods 77–78:92–103

Tables

Table 1. Demographics and Clinical Features in *PTEN* Positive or *PTEN* Negative NPC Patients

Characteristics		All patients (n=245) n (%)	*PTEN* positive (n=214) n (%)	*PTEN* negative (n=31) n (%)	p
Age (years)	Median	49	49	48	0.4254
	Range	21-77	21-77	31-72	
Gender	Male	185 (75.51)	160 (74.77)	25 (80.65)	0.6551
	Female	60 (24.49)	54 (25.23)	6 (19.35)	
T stage	1	5 (2.04)	4 (1.87)	1 (3.23)	**0.0421**
	2	63 (25.71)	59 (27.57)	4 (12.90)	
	3	114 (46.53)	102 (47.66)	12 (38.71)	
	4	63 (25.72)	49 (22.90)	14 (45.16)	
N stage	0	12 (4.90)	12 (5.61)	0 (0)	**0.0054**
	1	51 (20.82)	50 (23.36)	1 (3.23)	
	2	109 (44.48)	95 (44.39)	14 (45.16)	
	3	73 (29.80)	57 (26.64)	16 (51.61)	
M stage	0	229 (93.47)	204 (95.33)	25 (80.65)	**0.0081**
	1	16 (6.53)	10 (4.67)	6 (19.35)	
AJCC Stage	II	16 (6.53)	15 (7.01)	1 (3.26)	**0.0072**
	III	120 (48.98)	110 (51.40)	10 (32.23)	
	IV A	93 (37.96)	79 (36.92)	14 (45.16)	
	IV B	16 (6.53)	10 (4.67)	6 (19.35)	
Pathological Type	Undifferentiated non-keratinized carcinoma	216 (88.16)	191 (89.25)	25 (80.65)	0.3678
	Differentiated non-keratinized carcinoma	25 (10.20)	20 (9.35)	5 (16.13)	
	Keratinizing squamous cell carcinoma	4 (1.64)	3 (1.40)	1 (3.22)	

EBV	Positive	174 (70.02)	149 (69.63)	25 (80.65)	0.2893
	Negative	71 (28.98)	65 (30.37)	6 (19.35)	
PFS	Median	9.5	10.0	8.5	**0.0316**
	Range	3.0-29.5	0.5-29.5	3.0-23.0	

Significant correlations are highlighted in bold. AJCC= American Joint Committee on Cancer; EBV= Epstein-Barr virus; PFS=progression-free survival.

Table 2. *PTEN* Expression Revealed by DCE-MRI

	K^{trans} (min^{-1})	K_{ep} (min^{-1})	V_e	V_p
***PTEN* positive**	0.837±0.583	1.628±0.704	0.459±0.214	0.141±0.131
***PTEN* negative**	1.275±0.526	2.149±0.686	0.458±0.222	0.170±0.115
***P* (Mean comparison)**	**<0.001**	**<0.001**	0.6561	0.0735
Correlation coefficient (ρ)	-0.290	-0.241	-0.003	-0.115
***P* (Spearmen correlation)**	**<0.001**	**<0.001**	0.963	0.073

Significant correlations are highlighted in bold.

Figures

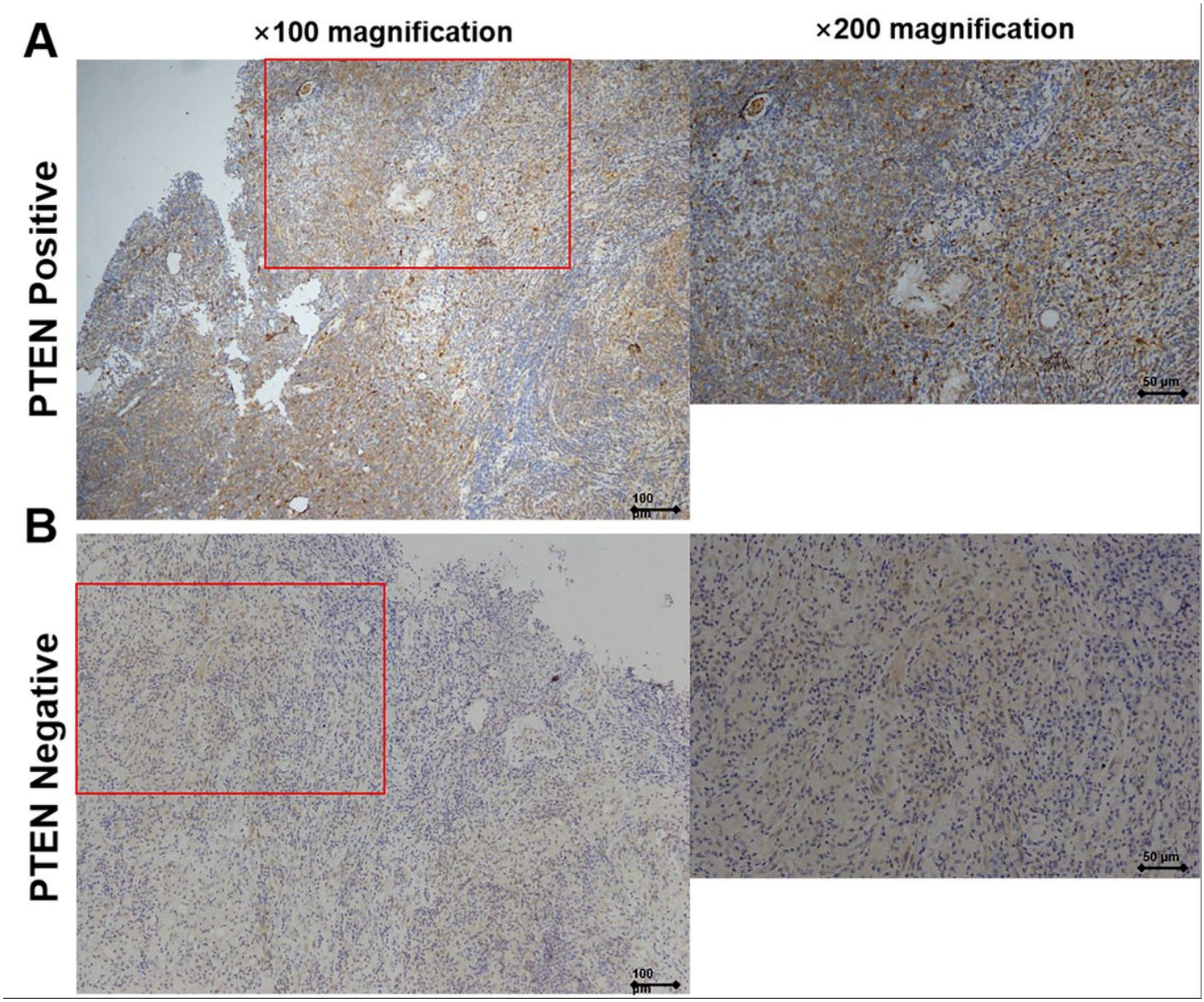

Figure 1

Histology of PTEN positive (A) and negative (B) expression (The left image*100 magnification, and the right image*200 magnification). Cells' nucleus/cytoplasm stained in yellow-brown, are positive for PTEN. The other cells are PTEN negative.

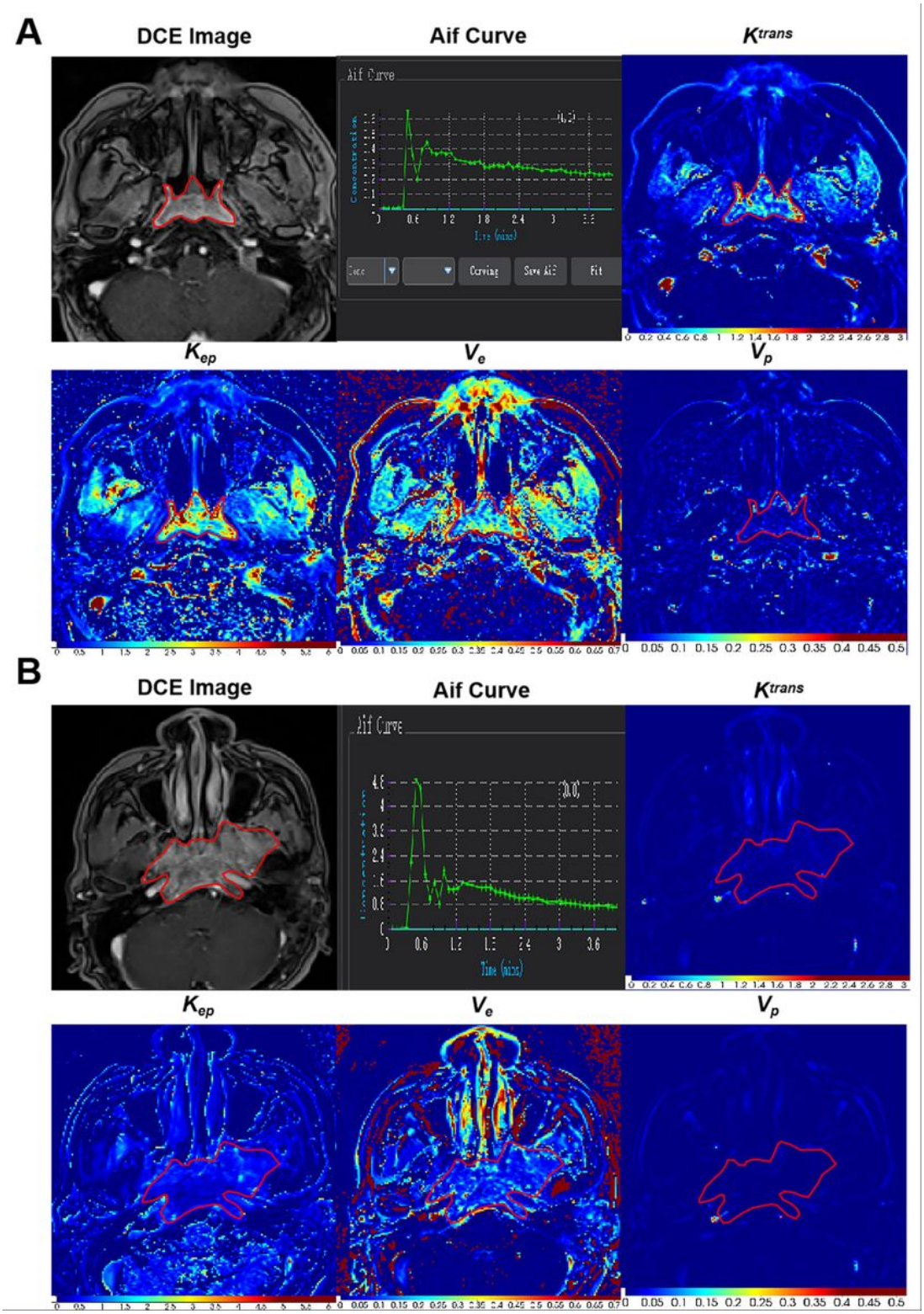

Figure 2

Typical DCE examples of the different expression levels of PTEN in NPC patients. PTEN positive (A) vs. PTEN negative expression (B). A showed the images of a 34-year-old male from the PTEN positive group with an IV4-stage NPC tumor. Ktrans (0.089), Kep (0.466), Ve (0.263), and Vp (0.008) were derived from DCE Toft's model. B showed the images of a 48-year-old male from the PTEN negative group with a V-

stage NPC tumor. Ktrans (1.542), Kep (3.025), Ve (0.154), and Vp (0.387) were derived from DCE Toft's model.

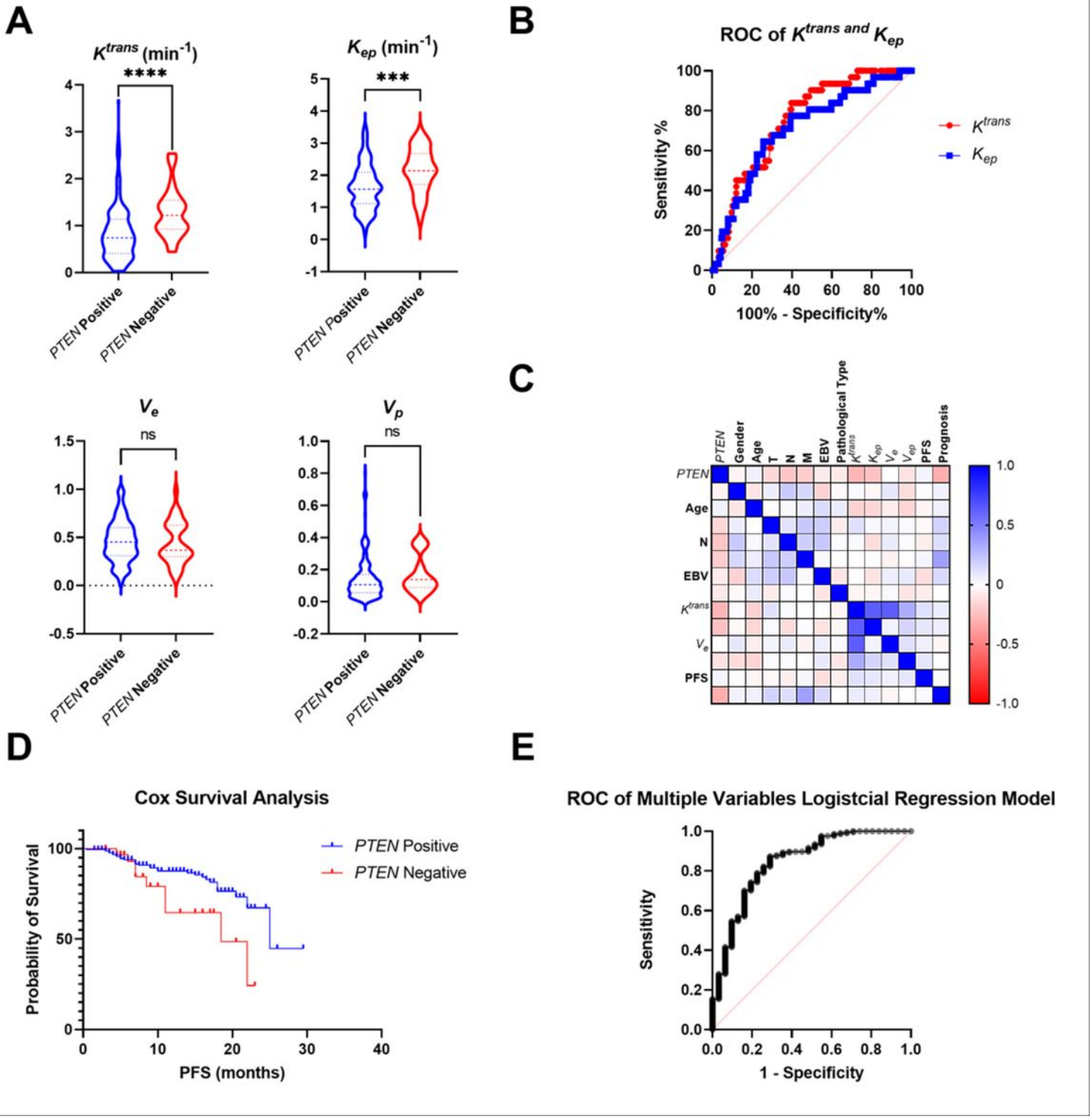

Figure 3

A. Comparison of DCE parameters between PTEN positive and PTEN negative group. There was a significant difference in Ktrans and Kep between PTEN positive and PTEN negative expression. B. ROC analysis showed Ktrans distinguishing PTEN positive from negative with an AUC of 0.752 (95% CI, 0.674-

0.829) and Kep with an AUC of 0.629 (95% CI, 0.524-0.734). C. Spearman correlation analysis for all the clinical features and DCE parameters. T, N, M stage, Ktrans, Kep, and prognosis status show significant correlated with PTEN expression. D. The Cox survival analysis showed the PTEN negative group has a significantly shorter PFS than PTEN positive group. E. The multiple variables logistic regression model has a good performance in detecting PTEN expression with an AUC of 0.843 (95% CI, 0.762-0.924). * P < 0.05; ** P < 0.01; *** P < 0.001; **** P < 0.0001